AeroBest 2025
Lisboa, 22–24 April 2025

DEFORMATION STRATEGIES IN FUSELAGE AERODYNAMIC SHAPE OPTIMIZATION USING PAYLOAD VOLUME CONSTRAINTS

Luís D. Pinheiro[1,2]*, Nuno M. B. Matos[1,2] and André C. Marta[2]

1: Research and Development
Tekever UAS
Rua das Minas, 2, 2500-750 Caldas da Rainha, Portugal
{luis.pinheiro, nuno.matos}@tekever.com, https://www.tekever.com

2: IDMEC
Instituto Superior Técnico
Universidade de Lisboa
Av. Rovisco Pais, 1, 1049-001 Lisboa, Portugal
{luis.pinheiro, andre.marta}@tecnico.ulisboa.pt, https://mdo.tecnico.ulisboa.pt

Abstract. *The usage of powerful optimization tools is becoming common in solving many engineering problems due to available computational resources and mature numerical algorithms. In this work, an adjoint-based high-fidelity aerodynamic shape optimization framework is used to manipulate a generic aircraft fuselage shape to minimize the total aerodynamic drag with specific payload volume constraints. The external fuselage shape is modified using the free-form deformation (FFD) technique to allow greater flexibility. The impact of using different deformation strategies applied to the displacement of FFD control points is studied, including displacements along the normal direction, the transverse axis directions, and cambering along the longitudinal axis direction. It is demonstrated that the combination of flexible control point displacement in multiple FFD box cross-section planes together with a streamwise cambering can produce a very significant drag reduction, in excess of 40% compared to the selected baseline shape, while still satisfying volume constraints to account for internal or protruding payloads.*

Keywords: aircraft design, gradient-based optimization, adjoint method, free form deformation, high-fidelity analysis, aerodynamic performance

1 INTRODUCTION

In recent years, the aviation industry has been expanding to more diverse solutions, proposing novel aircraft configurations and shapes. In addition, Unmanned Aerial Vehicles (UAVs) have been pivotal in multiple areas, such as agriculture, warfare and commodities built into our society [1–3]. Because of this growing market, aircraft shape optimization plays a crucial role in enhancing aerodynamic efficiency, payload distribution, structural integrity and overall flight performance. As this industry keeps evolving towards high-performance and efficient designs, the optimization of fuselages becomes critical.

Although traditional fuselage designs often present challenges related to drag reduction, weight minimization, and integration of different payloads, such as radars, gimbals or other components with random geometries, Computational Fluid Dynamics (CFD) and Multidisciplinary Design Optimization (MDO) [4] have enabled engineers to push the boundaries of fuselage designs, resulting in significant performance improvements [5–7]. Fuselage optimization is a critical area of modern aircraft design that has a direct influence on aerodynamic efficiency, structural stability, and operational flexibility [5, 8, 9]. Reducing parasitic drag [10], which accounts for a huge percentage of an aircraft's total aerodynamic drag, is one of the main targets in fuselage design. Through fuselage shape optimization, designers can have maximum control over airflow, which enables more efficient intersections with wings and tails, which in turn allows for innovative constructions with high aerodynamic performance [5]. Also, the ability to accommodate random and modular payload configurations efficiently is another critical factor in modern aircraft design, particularly in the UAV industry [11]. Unlike manned aircraft, UAVs do not require pressurized cabins, which offers greater design freedom in shape, weight distribution, and internal component layout. Therefore, fuselage shape optimization potentially offers greater performance gains while being flexible enough to accommodate a range of mission profiles.

In this work, gradient-based techniques will be used to guarantee rapid convergence to an optimized fuselage configuration, as demonstrated in similar cases [12, 13]. The gradients of the cost and constraint functions will be efficiently calculated using the adjoint method [14], making the computational cost independent of the number of design variables, which is expected to be large in shape optimization.

Various parametrization strategies will be explored to efficiently optimize the fuselage shape for best aerodynamic performance for a simple generic fuselage. For this, the free-form deformation (FFD) method, which is one kind of geometry modification technique that parametrizes shape perturbation instead of the shape itself used in aircraft design optimization, will be used [15]. The deformation process will include deformations along the fuselage axis, radial deformations, and deformations along the normals of the control points of the Free-Form Deformation (FFD) box. In addition, local shape modifications, such as cambering specific areas, mainly around the nose or tail area, will be analyzed.

In order to ensure practical feasibility, volume constraints will be included in the optimization framework. These constraints are important to preserve payload volume, as well as internal component allocation, and to avoid aggressive shape distortions that would compromise the aircraft's functional requirements [16, 17]. Through the imposition of volume preservation in key fuselage regions, the optimization will balance aerodynamic gains with real-world design constraints.

2 SHAPE DEFORMATION MODELING

Shape deformation modeling is an important technique in aerodynamic optimization to drive precise geometric deformation to achieve desired performance goals. Various techniques can be employed, including basis vector, domain element, discrete, analytical, Free-Form Deformation (FFD), partial differential equation (PDE), polynomial and spline, and Computer-Aided Design (CAD) [18–20]. FFD and CAD-based approaches are very efficient for complex problems [21]. Nevertheless, CAD systems still have problems parameterizing complex geometries and generating suitable grids for automatic simulations [21], making FFD a promising solution.

The FFD method has been successfully applied in aircraft design problems, such as helicopter fuselage optimization [22], manipulating the control points within a volume to generate smooth deformations. Other examples can be found in the works of Ekici and Juniper [23], Zhao et al. [24]. Moreover, this strategy also supports alterations in triangulated surface nodes and structure surface meshes along with a decrease in design variables [25]. Though FFD is not said to control any part of the design directly, it is still quite effective where solutions to aerodynamics entail huge displacements. The framework used in this study, Mach-Aero [26], incorporates the FFD method [27, 28].

2.1 Fuselage Deformation using FFD

The first study case is illustrated in Fig. 1, where the CFD mesh of the simplified fuselage used in the preliminary studies within the corresponding FFD box is shown. This arrangement sets the baseline geometry, allowing systematic modifications of the fuselage geometry by displacing control points within the FFD box, which subsequently rebuilds the 3D computational mesh.

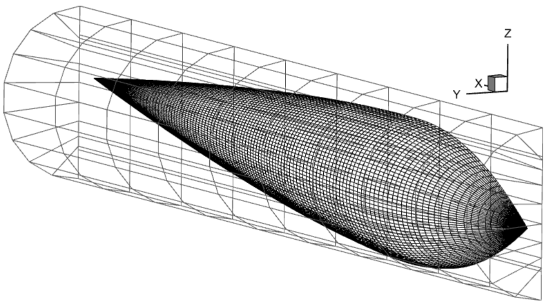

Figure 1: Simplified fuselage CFD mesh with the initial FFD box.

The FFD box resolution, in terms of number of control points, plays an important role in the flexibility of the deformations and must align with the optimization study's goals. A coarser grid with a few control points has a good capacity for preserving global deformations and, therefore, it is well suited to initial design and shape optimization at scales like the one shown in Fig. 2a. However, a finer grid with more control points, as illustrated in Fig. 2b, provides room for local control. The balance between shape degrees of freedom and computational cost has to be treated with great caution when introducing additional shape design variables [29].

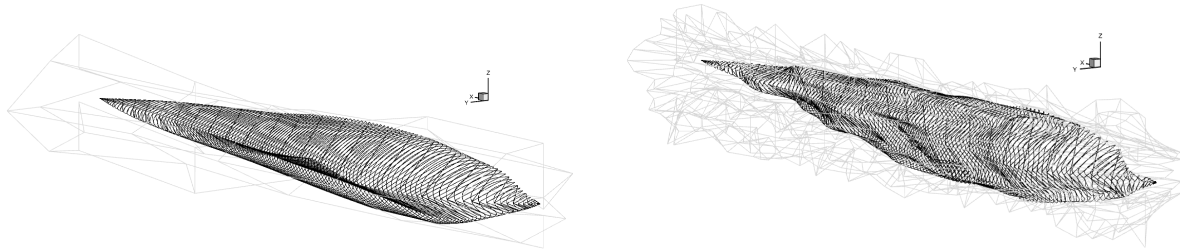

(a) Coarse FFD box.   (b) Fine FFD box.

Figure 2: FFD box modeling.

2.2 Strategies for FFD Control Point Displacements

The parametrization of the FFD box and, hence, of the fuselage shape, can be done by several strategies with different advantages, depending on the optimization problem, as illustrated in Fig.4 for three different strategies.

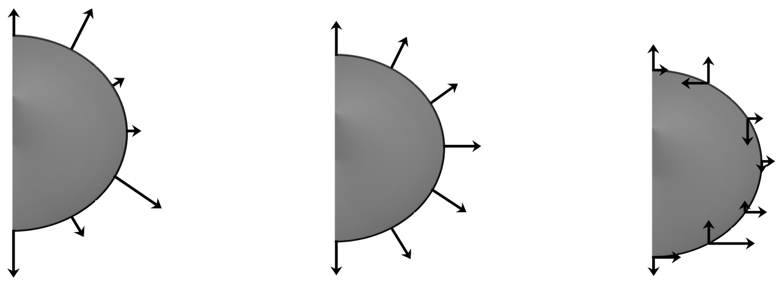

(a) Normal direction   (b) Radial direction   (c) Y-, Z-direction

Figure 3: Different deformation strategies.

The first parametrization strategies (Fig.3a) uses the normal directions of the FFD box points, hence the deformations are defined in different directions based on the FFD box and fuselage geometry, offering flexibility to the optimizer. However, this strategies might produce less intuitive deformations for certain geometries, as the control points will move in different directions.

The second parametrization strategies (Fig.3b) uses radial deformations, making necessary the definition of a reference axis. By adjusting the fuselage's dimensions through scaling functions, this strategies makes it possible to expand or contract selected areas. However, for the present study, it was not as effective since the goal was to reshape the geometry in study and not reduce its size [28].

The last parametrization strategies (Fig.3c) performs deformations along the X, Y, and Z axes. It makes it convenient to use when scaling, stretching, or compressing along the axes, since it provides controlled shape variation in specific directions and provides the user with a clear understanding of the optimizer choices.

In addition to the three strategies described, it is also possible to define specific regions of the fuselage to be parametrized, spatially restricting the deformation region, with the use of a subset of control points defined by Point Selection. This gives the ability to deform different parts of the fuselage using distinct functions with different values, as observed in Fig. 4, which demonstrates how it is possible to reshape only certain parts of the geometry in study using the normal vectors of the FFD box.

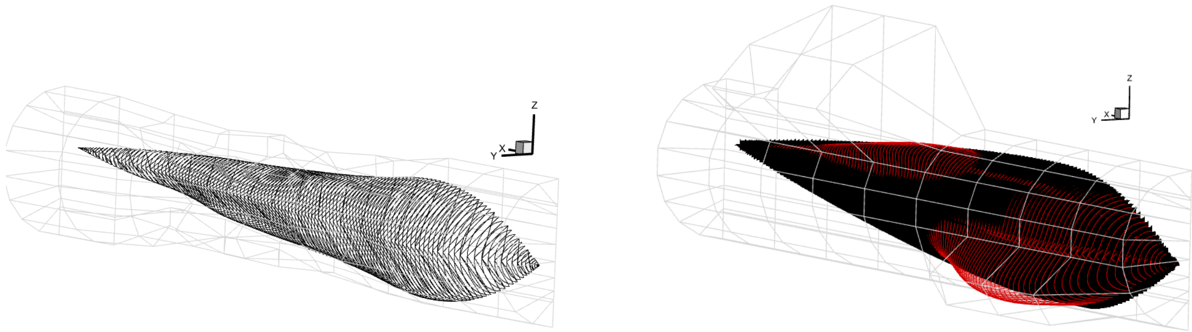

(a) Specific Volume (b) Specific Points

Figure 4: Specified deformations in the FFD box.

2.3 Cambered Fuselages

While the strategies presented in Sec.2.2 offer great freedom, the desire to employ a well-defined engineering parameter led to the definition of fuselage camber. Although fuselages are typically aerodynamically designed to have little contribution to total lift, that can be obtained by cambering the tail and nose sections [30, 31]. Such parametrization of a fuselage using camber was defined in the current framework using a quadratic function, as plotted in Fig. 5a, being the quadratic coefficient used later as a design variable during optimization. An example of such deformation can be observed in Fig. 5b, where both nose and trail camber have been added, where the fuselage length was normalized for the application of the quadratic function along its entire length.

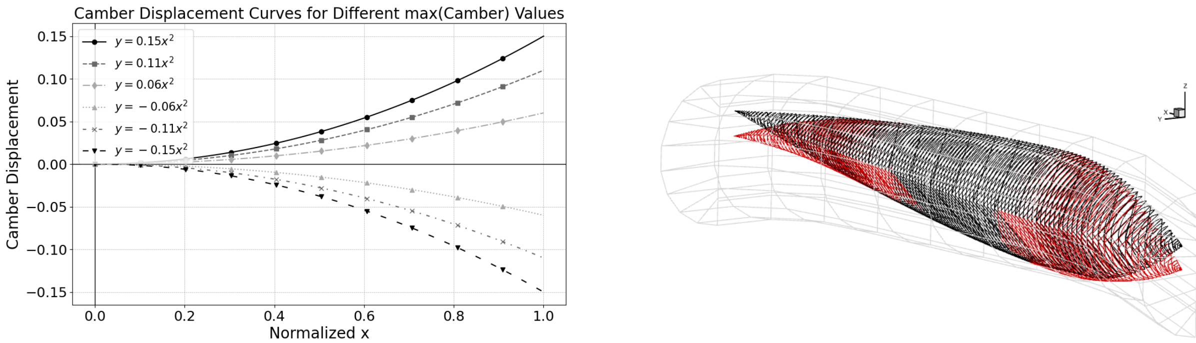

(a) Quadratic camber functions. (b) Nose and tail fuselage deformation.

Figure 5: Camber parametrization.

This strategy can be further customized by selecting only certain FFD control points to restrict the deformation to only certain fuselage regions, namely by deforming the nose and tail with different independent curvatures. This selective approach can potentially enhance lift and stability adjustments while minimizing unwanted aerodynamic disturbances, particularly at intersection regions (with wing or tail).

2.4 Volume Constraints

To prevent that the fuselage shape deformations during the optimization still lead to internal fuselage volumes that account for specific payload, such as radar or fuel tank, volume and triangulated surface constraints must be implemented [16].

On one hand, the volume constraint enforces volumes into the fuselages that prevent excessive deformations that could comprise the necessary payload volume. On the other hand, the triangulated surface constraint uses an STL file format to define a given 3D shape that must be encapsulated by the fuselage shape, thus limiting the shape deformation during optimization. The latter constraint facilitates the integration of payloads into aerodynamic problems, giving more freedom in the optimization. Fig. 6 illustrates an example of a possible internal (a) or partially external (b) payload shape (sphere) defined using an STL file.

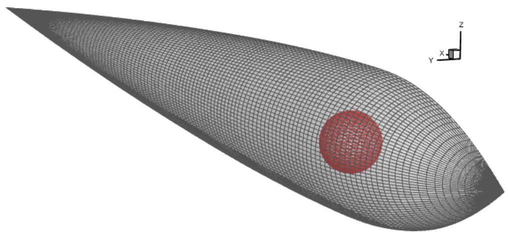

(a) Internal payload.

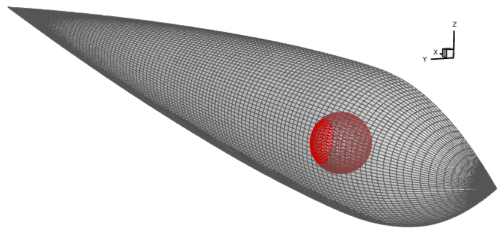

(b) Partially external payload.

Figure 6: Fuselage volume constraint (in red) defined by triangulated surface.

3 FUSELAGE SHAPE OPTIMIZATION

The baseline fuselage shape shown in Fig.1 will be used as a starting point for the aerodynamic optimization problem aimed at minimizing the drag coefficient, posed in standard form as

$$\begin{array}{ll} \underset{\boldsymbol{x}}{\text{minimize}} & C_D(\boldsymbol{x}) \\ \text{subject to} & \mathrm{KS}_{\mathrm{geom}} \leq 0 \end{array} , \tag{1}$$

where $\boldsymbol{x}$ is the vector of all design variables (DVs) used in each case, which include the coordinates of the FFD control points and/or the amplitude of the camber function. The constraint function $\mathrm{KS}_{\mathrm{geom}}(\boldsymbol{x})$ represents an aggregated geometric constraint based on the Kreisselmeier–Steinhauser (KS) function, which provides a smooth and conservative approximation of the maximum deviation between triangulated surfaces [16]. All optimization cases were performed in the MACH-Aero framework [14], using ADFlow [32] to evaluate the aerodynamic performance. The gradient-based SLSQP algorithm was used with a convergence tolerance of 10^{-6} and with a maximum of 1000 iterations.

The fuselage operating condition represented a flight at a speed of 34 m/s at Standard Sea Level, with zero angle of attack (flow aligned with X-axis).

The different deformation strategies explained in Sec.2.2 are evaluated and theirs effectiveness compared. The strategies individual considered are normal-based deformations (Fig.7a), directional deformations along a specific axis Y (Fig.7b), Z (Fig.7c) or both (Fig.7d), and cambered fuselage deformations (Figs.9a, 9b and 9c). The combined camber and normal vectors (Fig.9d) or Y-/Z-directions (Fig.9e) are also studied. Lastly, the effect of volume constraints in the optimal fuselage shape is also studied for both internal and protruding objects (Fig.10). The detailed discussion of all results is included in Sec.4.

3.1 Selected FFD Points

The first set of studies included the normal-based, and the (Y- and Z-) direction-based deformation parametrization strategies. Each strategy required specific considerations to ensure the stability of the optimization process, particularly to prevent the generation of invalid geometries, such as negative volumes, which would cause the mesh to fail and compromise the optimization. The resulting optimized fuselage shapes are illustrated in Fig. 7.

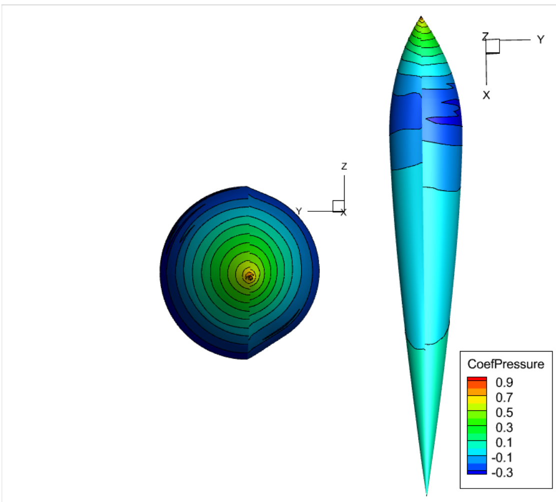

(a) Normal vectors

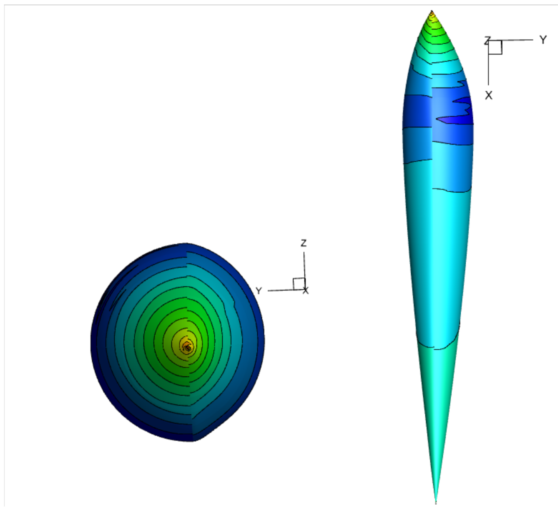

(b) Y direction

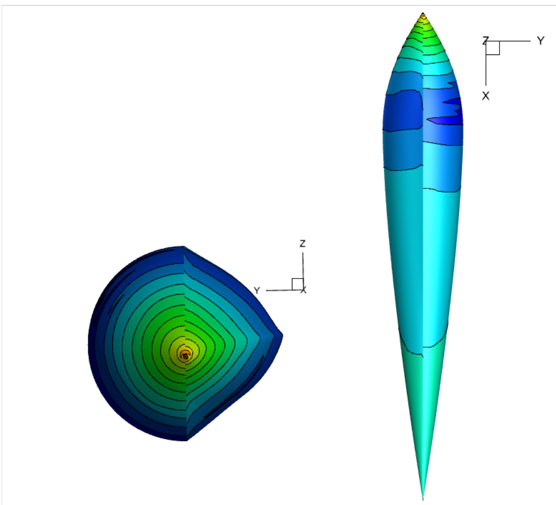

(c) Z direction

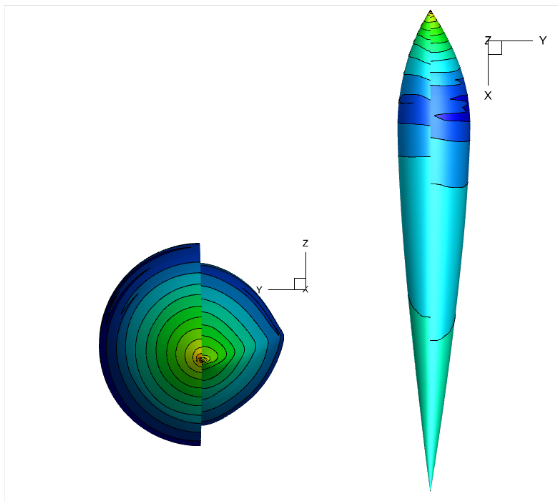

(d) Y and Z directions

Figure 7: Optimal shapes using different parametrization strategies.

For the normal-based deformations, Fig. 7a, it was necessary to carefully select which regions of the FFD box could be parametrized. Points located near the symmetry plane ($y = 0$) were excluded, as their displacements could easily produce negative CFD mesh volumes and, subsequently, make the optimization process to fail. Additionally, the points near the edges of the fuselage, specifically at the nose and tail, were also frozen to prevent geometric inconsistencies at the edges, avoiding similar problems. Furthermore, the freedom given to the FFD points was kept relatively small to avoid, again, the risk of generating invalid mesh volumes. These limitations directly impacted the optimization results, as seen in the corresponding figures and data summarized in Tab.1.

In contrast, the directional deformation strategy, which deforms the geometry along the Y- and Z-axis, was generally easier to control. As expected, the freedom given to the FFD points could be increased without immediately risking mesh failures in these cases. However, this strategy tended to excessively deform certain regions of the fuselage, particularly near the tail, creating irregular geometries, almost like a twist or warp in these regions, as observed in Fig.8. Similar to the normal-based strategy, the points at

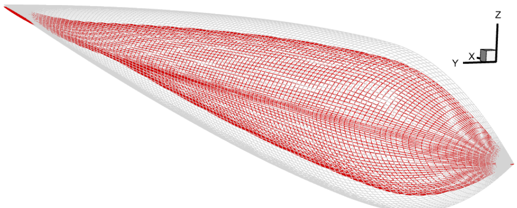

Figure 8: Irregularities encountered using the directional deformation method

the fuselage leading and trailing edges were kept fixed to avoid negative mesh volumes, which limited the flexibility of the surrounding regions, thus aggravating the localized deformations observed.

3.2 Camber Function

The second set of studies was conducted to identify the benefits of adding camber to the fuselage. The precautions when setting up these cases are primarily related to avoid creating mismatches in the intersection regions with components such as wings or tails. To address this issue, freedom was given only at specific longitudinal (X-axis) intervals that excluded intersection regions to prevent the aforementioned problems. Three different cases were tested, applying the camber function only in the nose region, tail region, or both, which produced the optimal shapes shown in Fig. 9,

3.3 Combined Deformation Strategies

The last two studies include the combination of the camber function with the normal- or direction-based strategy. The resulting fuselage shapes are shown in Figs.9d and 9e, respectively.

3.4 Volume Constraints

To complete the study, the Triangulated Surface Constraint was tested with the same different shape deformation strategies. The same 3D object, a sphere, was used in these cases to represent any given payload. Two different object locations were experimented: the object inside the baseline fuselage and partially outside, protruding the baseline fuselage shape.

The cross-section of the resulting optimal fuselage shapes obtained with the different deformation strategies, passing through the object, are illustrated in Fig. 10. The so-

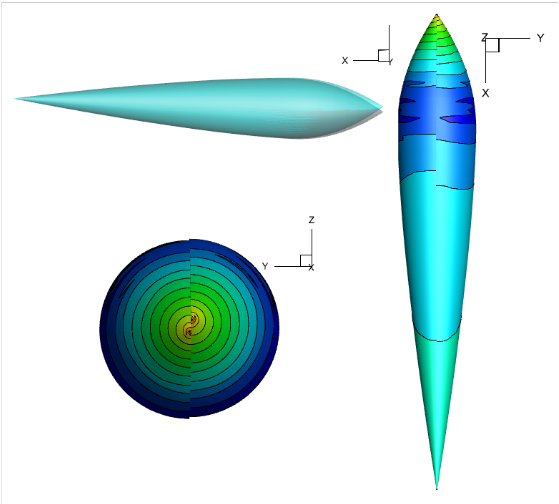

(a) Restricted to nose.

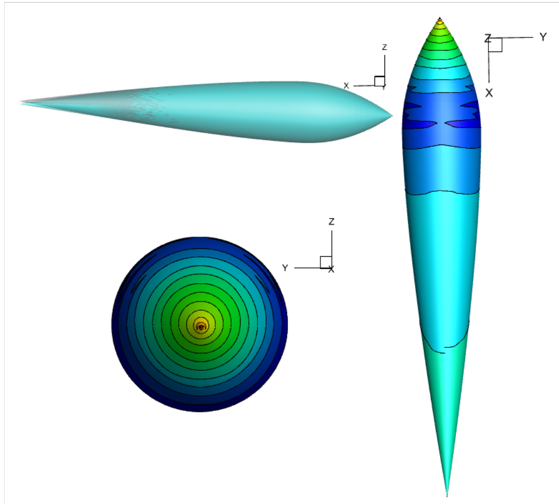

(b) Restricted to tail.

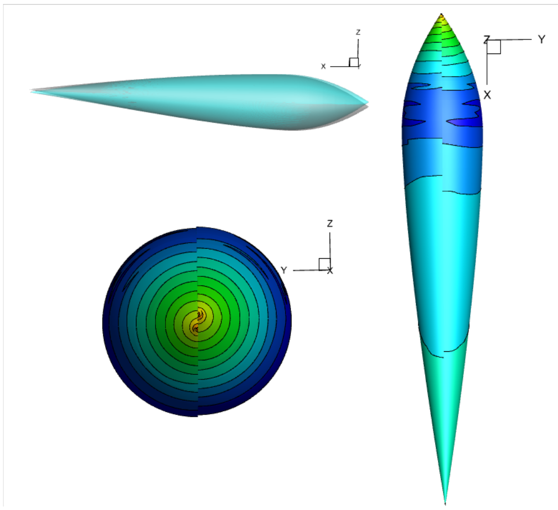

(c) Restricted to nose and tail.

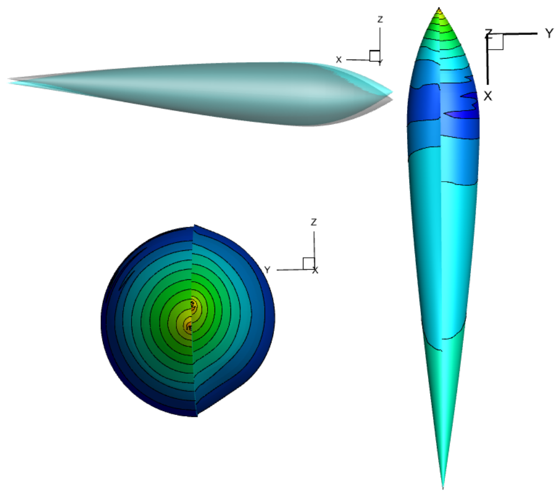

(d) Camber combined with normal vectors.

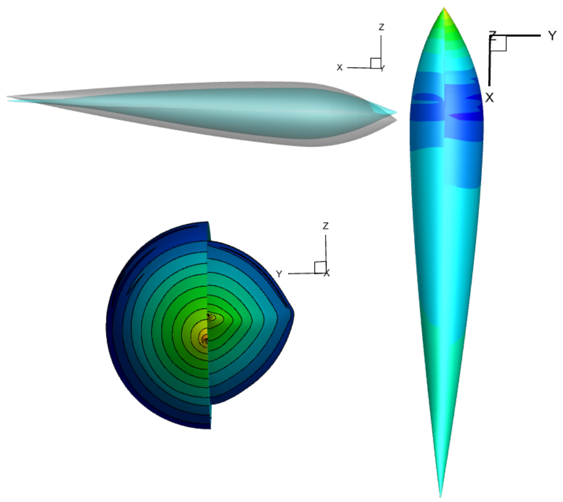

(e) Camber combined with Y and Z directions.

Figure 9: Optimal shapes with camber deformation strategy.

lutions to the problems with the object inside the baseline fuselage include: combined camber and normal-based deformations (Fig.10a), combined camber and deformations along the Y- and Z-axes (Fig.10b), and deformations only along normal-vectors of the FFD box (Fig.10c). In addition, the cases with the object initially protruding the baseline fuselage are shown in Figs.10d and 10e, using normal-vectors, and combined with z-axis deformation, respectively.

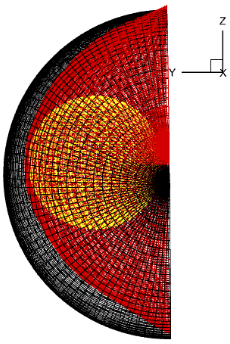

(a) Camber + normal vectors deformations with sphere inside fuselage.

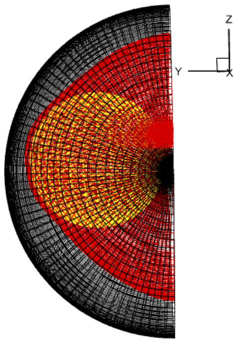

(b) Camber + (Y and Z) deformations with sphere inside fuselage.

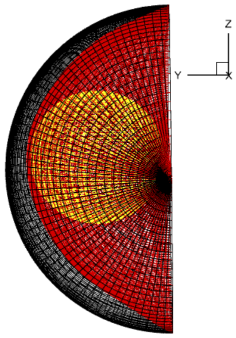

(c) Parametrization using normals of FFD points with sphere inside fuselage.

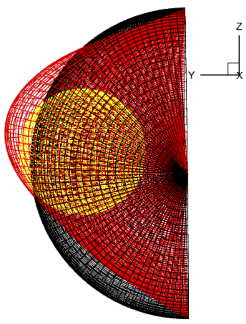

(d) Parametrization using normals of FFD points.

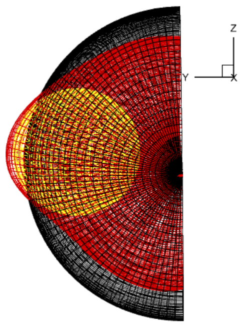

(e) Parametrization along Z-axis, combined with normal vectors of FFD points.

Figure 10: Optimal shapes using the triangulated surface constraint.

As attested in Fig. 10, each of the presented cases made the optimizer manipulate the FFD control points in different ways to ensure that the fuselage could envelop the payload (sphere).

The main differences encountered between the cases shown in Figs.10d and 10e arise from the variation in the selected points. While deforming the shape using the normal vectors of the FFD box points, it was necessary to exclude points near the plane of symmetry ($y = 0$) to prevent mesh issues and negative volumes, which caused the differences. To mitigate this problem, it was given freedom to these points along the Z axis in the second case, which visibly improved the design, as the fuselage was able to shrink near the symmetry plane, resulting in a smoother and more effective deformation.

Finally, the differences between parameterizations with and without the triangulated surface constraint can be observed in Fig.11, where two different cases are illustrated: combined camber and normal-based deformations (Fig.11a) and camber with deformations along the Y and Z axes (Fig.11b), both showing optimized fuselages taking (red) or not (black) into consideration the triangulated surface constraint. It is clear that, despite using the same parameter values, the resulting shapes differ significantly. It is also worth noting that, for the optimized fuselages (black), the optimal design variable values reached their imposed lower bounds, which suggests that the optimizer could have further reduced the fuselage size in the absence of these.

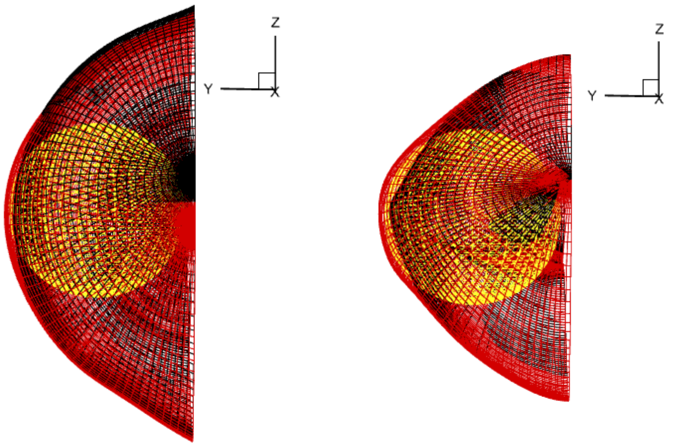

(a) Camber + normal vectors deformations.

(b) Camber + (Y and Z) deformations.

Figure 11: Comparison of optimal shapes with (red) or without (black) triangulated surface constraint.

4 DISCUSSION OF RESULTS

The drag reduction obtained for each of the different deformation strategies studied in Sec.3 is listed in Tab.1.

Through the analysis of optimal shapes presented in Sec.3 and the aerodynamic performance gains presented in Tab.1, it is possible to assess about the effectiveness of the different shape parametrization strategies proposed. Notice, however, that these optimal shapes were obtained from problems that differed slightly in terms of design variable bounds to overcome mesh morphing fails, as such, the comparisons might not extrapolate directly to other fuselage geometries.

In the cases with the deformation parametrization along the normal vectors of the FFD box points, the optimized shapes exhibited fewer irregularities and a more stable CFD mesh morphing, leading to a nearly 17% drag reduction for either the unconstrained and internal volume constrained cases, but less an expressive 7% reduction in the protruding payload case. However, this strategy revealed to be relatively limited and not well adapted to arbitrary fuselage shapes.

Looking at the strategies using deformations along the Y- and Z-directions, they exhibited a much greater drag reduction compared to the normal direction strategy. The Y-direction only strategy, corresponding the lateral fuselage deformations led to consid-

Table 1: Optimization deformation strategy studies and corresponding drag coefficient reduction.

Parametrization strategy	**Constraints**	**Opt. shape**	**Min C_D**	ΔC_D
(baseline)			0.0189	ref
Normals	None	Fig.7a	0.0161	-16.6%
Y-axis	None	Fig.7b	0.0155	-21.6%
Z-axis	None	Fig.7c	0.0168	-11.7%
(Y, Z)-axis	None	Fig.7d	0.0114	-40.4%
Nose Camber	None	Fig.9a	0.0185	-2.1%
Tail Camber	None	Fig.9b	0.0185	-2.1%
(Tail, Nose) Camber	None	Fig.9c	0.0184	-2.3%
Camber + Normals	None	Fig.9d	0.0161	-17.1%
Camber + (Y, Z)-axis	None	Fig.9e	0.0133	-41.6%
Camber + Normals	TS (IS)	Fig.10a	0.0162	-16.9%
Camber + (Y, Z)-axis	TS (IS)	Fig.10b	0.0135	-39.8%
Normals	TS (IS)	Fig.10c	0.0162	-16.4%
Normals	TS (IntS)	Fig.10d	0.0176	-7.0%
Normals + Z-axis	TS (IntS)	Fig.10e	0.0155	-21.3%

TS = Triangulated Surface, IS = Internal Sphere, IntS = Intersected Sphere.

erably better shapes compared to the Z-direction only strategy, and, unsurprisingly given the greater deformation freedom, the combination of both Y- and Z-direction deformations led to an impressive 40% drag reduction.

When considering the deformation using the camber function alone, little impact in the aerodynamic performance was obtained, limited to about 2% reduction in drag, regardless of the regions manipulated (nose, tail or both). However, tuning the fuselage camber has been shown to improve the airflow going through the fuselage to the wing [30, 31], as should not be discarded in more complex cases.

The combination of the camber deformation with the simultaneous Y- and Z-direction deformation resulted in the best overall unconstrained fuselage shape, which exhibited a massive 41.6% drag reduction compared to the baseline. However, some cautions regarding the optimized shape must be taken into consideration since some irregularities were created during the optimization. This combined strategy also produced the best aerodynamic shape for the constrained case with internal payload, with almost 40% drag reduction.

In future studies, to mitigate the referred problems seen in Fig.8, it might be beneficial to make some modifications near the tail region of the fuselage, such as adding a volume constraint might prevent the formation of torsion or warping. Another way to prevent these irregularities could be to incorporate a parametrization strategy, such as those discussed in this study, which, when combined with the Point Selection method, might allow for greater flexibility and deformation control in the affected region.

Referring the the protruding payload cases, only the deformation strategy along the normal vectors was considered to prevent irregular deformations in the fuselage while integrating the triangulated surface constraint with the sphere intersected in the main body. However, in this study, and when comparing the cases represented by Figs.10d and

10e, the normal direction deformation only case led to a 7% drag reduction while the combination with the Z-direction deformation increase the reduction significantly to over 21%, mostly due to the impact of the manipulation of the FFD points near the fuselage vertical symmetry XZ-plane.

5 CONCLUSIONS

Several parametrization strategies for fuselage deformation in aerodynamic shape optimization were proposed, tested and compared. This allowed an understanding of the characteristics of each strategy and how they can be applied in more complex design problems.

Drag reduction ranging from 2.1% to 41.6% were observed, depending on the case study considered. Despite the directional parametrization leading to greater drag reduction, the parametrization along the normal vectors of the FFD box points should not be excluded when opting for a deformation strategy. This strategy combined with a deformation along the vertical Z-axis have produced good results as well, with the added benefit of reducing the surface irregularities if the DV bounds are properly set.

This work highlighted the importance of selecting appropriate parametrization strategies based on both aerodynamic performance and payload constraints (internal to the fuselage or partially protruding). The triangulated surface constraint proved to be a powerful tool in constraining an aerodynamic problem, offering multiple applications to handle the payload positioning and volume required.

While this study focused on specific implementations, future research should explore the impact of varying constraint parameters, such as spatial tolerance [16].

ACKNOWLEDGEMENTS

The authors would like to thank Tekever UAS for supporting the production of this article by offering all the needed data to successfully produce the analyses here shown.

The third acknowledges Fundação para a Ciência e a Tecnologia (FCT) for its financial support via the project LAETA Base Funding (DOI: 10.54499/UIDB/50022/2020).

REFERENCES

[1] K. K. Reddy, S. K. Basha, B. Naveen, and K. Abhilash. The game-changing role of drones in agriculture. *Agri Express*, 02, May 2024. ISSN 2584 - 2498.

[2] Ö. Ö. Kanat. The significance of unmanned aerial vehicles (uavs) in strategic contexts. *Anadolu Strateji Dergisi*, 5(2):75–87, 2023.

[3] H. Shakhatreh, A. H. Sawalmeh, A. Al-Fuqaha, Z. Dou, E. Almaita, I. Khalil, N. S. Othman, A. Khreishah, and M. Guizani. Unmanned aerial vehicles (uavs): A survey on civil applications and key research challenges. *IEEE Access*, February 2019.

[4] J. R. R. A. Martins and A. B. Lambe. Multidisciplinary design optimization: A survey of architectures. *AIAA Journal*, 51(9):2049–2075, 2013. doi:10.2514/1.J051895.

[5] S. Rohani and A. Jahangirian. Multi-objective aerodynamic optimization of a civil aircraft fuselage. *ICAS, Shanghai, China*, pages 1–6, 2021.

[6] A. Dhara, A. Majumder, N. E. Kumar, M. Dhanunjay, L. T. Dhanumjaya, and J. Muruga Lal Jeyan. Design optimization to minimize wake of wide-body transport aircraft. *Journal of Engineering Research*, 12(2):200–209, 2024. ISSN 2307-1877. doi:https://doi.org/10.1016/j.jer.2023.08.014.

[7] J. R. Martins. Aerodynamic design optimization: Challenges and perspectives. *Computers & Fluids*, 239:105391, 2022. ISSN 0045-7930. doi:10.1016/j.compfluid.2022.105391.

[8] J. Welstead, B. Reitz, and G. Crouse. Modeling fuselage aerodynamic effects in aircraft design optimization. In *50th AIAA Aerospace Sciences Meeting Including the New Horizons Forum and Aerospace Exposition*, 01 2012. ISBN 978-1-60086-936-5. doi:10.2514/6.2012-394.

[9] J. Mieloszyk and T. Goetzendorf-Grabowski. Introduction of full flight dynamic stability constraints in aircraft multidisciplinary optimization. *Aerospace Science and Technology*, 68:252–260, 2017. ISSN 1270-9638. doi:10.1016/j.ast.2017.05.024.

[10] D. P. Raymer. *Aircraft Design: A Conceptual Approach.* AIAA Education Series. American Institute of Aeronautics and Astronautics, Inc., 2 edition, 2012. ISBN 0-930403-51-7.

[11] S. A. H. Mohsan, N. Q. H. Othman, L. Yanlong, M. Alsharif, and M. Khan. Unmanned aerial vehicles (uavs): Practical aspects, applications, open challenges, security issues, and future trends. *Intelligent Service Robotics*, 01 2023. doi:10.1007/s11370-022-00452-4.

[12] S. Roy and W. Crossley. Hybrid multi-objective combinatorial optimization technique with improved compatibility between ga and gradient-based local search. In *12th AIAA Aviation Technology, Integration, and Operations (ATIO) Conference and 14th AIAA/ISSMO Multidisciplinary Analysis and Optimization Conference*, September 2012. doi:10.2514/6.2012-5568.

[13] S. Khosravi and D. W. Zingg. A numerical optimization study on winglets. In *15th AIAA/ISSMO multidisciplinary analysis and optimization conference*, 2014. doi:10.2514/6.2014-2173.

[14] G. K. W. Kenway, C. A. Mader, P. He, and J. R. R. A. Martins. Effective adjoint approaches for computational fluid dynamics. *Progress in Aerospace Sciences*, 110: 100542, October 2019. doi:10.1016/j.paerosci.2019.05.002.

[15] J. Reid and P. He. *Free-Form Deformation (FFD).* DAFoam, February 2021. Accessed on January 25, 2025.

[16] B. J. Brelje, J. L. Anibal, A. Yildirim, C. A. Mader, and J. R. R. A. Martins. Flexible formulation of spatial integration constraints in aerodynamic shape optimization. *AIAA Journal*, 58(6):2571–2580, 2020. doi:10.2514/1.J058366.

[17] G. Burgreen and O. Baysal. Three-dimensional aerodynamic shape optimization of supersonic delta wings. In *5th Symposium on Multidisciplinary Analysis and Optimization*, September 1994. doi:10.2514/6.1994-4271.

[18] J. A. Samareh. Survey of shape parameterization techniques for high-fidelity multidisciplinary shape optimization. *AIAA Journal*, 39(5):877–884, 2001. doi:10.2514/2.1391.

[19] A. Hahn. Vehicle sketch pad: A parametric geometry modeler for conceptual aircraft design. In *48th AIAA Aerospace Sciences Meeting Including the New Horizons Forum and Aerospace Exposition*, 2010. doi:10.2514/6.2010-657.

[20] D. Rodriguez and P. Sturdza. *A Rapid Geometry Engine for Preliminary Aircraft Design*. American Institute of Aeronautics and Astronautics, January 2006. doi:10.2514/6.2006-929.

[21] J. A. Samareh. Aerodynamic shape optimization based on free-form deformation. *Collection of Technical Papers - 10th AIAA/ISSMO Multidisciplinary Analysis and Optimization Conference*, 6:3672–3683, 2004. doi:10.2514/6.2004-4630.

[22] M. Wentrup. An adjoint based optimization chain for complex helicopter fuselage parts using a free form deformation or cad based parameterization method. In *41st European Rotorcraft Forum*, September 2015.

[23] E. Ekici and M. P. Juniper. Adjoint based shape optimization for thermoacoustic stability of combustors using free form deformation. In *Turbo Expo: Power for Land, Sea, and Air*, volume 87943, page V03AT04A058. American Society of Mechanical Engineers, 2024.

[24] H. Zhao, J. T. Hwang, and J.-S. Chen. Open-source shape optimization for isogeometric shells using fenics and openmdao, 2024. URL `https://arxiv.org/abs/2410.02225`.

[25] N. R. Secco, J. P. Jasa, G. K. W. Kenway, and J. R. R. A. Martins. Component-based geometry manipulation for aerodynamic shape optimization with overset meshes. *AIAA Journal*, 56(9):3667–3679, 2018. doi:10.2514/1.J056550.

[26] MDO Lab. MDO Lab Mach-Aero Documentation. URL `https://mdolab-mach-aero.readthedocs-hosted.com/en/latest/`. Accessed: March 10, 2025.

[27] G. K. W. Kenway, G. J. Kennedy, and J. R. R. A. Martins. A CAD-free approach to high-fidelity aerostructural optimization. In *Proceedings of the 13th AIAA/ISSMO Multidisciplinary Analysis Optimization Conference*, Fort Worth, TX, September 2010. AIAA 2010-9231.

[28] H. M. Hajdik, A. Yildirim, E. Wu, B. J. Brelje, S. Seraj, M. Mangano, J. L. Anibal, E. Jonsson, E. J. Adler, C. A. Mader, G. K. w. Kenway, and J. R. r. a. Martins. pygeo: A geometry package for multidisciplinary design optimization. *Journal of Open Source Software*, 8(87):5319, 2023. doi:10.21105/joss.05319.

[29] L. A. Schwarz. Non-rigid registration using free-form deformations. Master's thesis, Technical University of Munich (TUM), May 2007.

[30] M. Z. bin Md Shah, M. R. bin Abu Bakar, and B. Basuno. The aerodynamics analysis on cambered fuselage model. In *Advances in Mechanical, Materials and Manufacturing Engineering*, volume 660 of *Applied Mechanics and Materials*, pages 492–497, 11 2014. doi:10.4028/www.scientific.net/AMM.660.492.

[31] K. D. Harris. An experimental investigation of the subsonic drag and pitching moment characteristics of slender cambered bodies with pointed noses and tails. Technical report, The College of Aeronautics, Cranfield University, September 1958.

[32] C. A. Mader, G. K. W. Kenway, A. Yildirim, and J. R. R. A. Martins. ADflow: An open-source computational fluid dynamics solver for aerodynamic and multidisciplinary optimization. *Journal of Aerospace Information Systems*, 17(9):508–527, Sept. 2020. doi:10.2514/1.I010796.